

## Accepted Manuscript

Highly efficient removal of trimethoprim based on peroxymonosulfate activation by carbonized resin with Co doping: performance, mechanism and degradation pathway

Yang Liu, Hongguang Guo, Yongli Zhang, Xin Cheng, Peng Zhou, Jing Deng, Jingquan Wang, Wei Li

PII: S1385-8947(18)31803-5  
DOI: <https://doi.org/10.1016/j.cej.2018.09.086>  
Reference: CEJ 19925

To appear in: *Chemical Engineering Journal*

Received Date: 26 June 2018  
Revised Date: 28 August 2018  
Accepted Date: 10 September 2018

Please cite this article as: Y. Liu, H. Guo, Y. Zhang, X. Cheng, P. Zhou, J. Deng, J. Wang, W. Li, Highly efficient removal of trimethoprim based on peroxymonosulfate activation by carbonized resin with Co doping: performance, mechanism and degradation pathway, *Chemical Engineering Journal* (2018), doi: <https://doi.org/10.1016/j.cej.2018.09.086>

This is a PDF file of an unedited manuscript that has been accepted for publication. As a service to our customers we are providing this early version of the manuscript. The manuscript will undergo copyediting, typesetting, and review of the resulting proof before it is published in its final form. Please note that during the production process errors may be discovered which could affect the content, and all legal disclaimers that apply to the journal pertain.



## Highly efficient removal of trimethoprim based on peroxymonosulfate activation by carbonized resin with Co doping: performance, mechanism and degradation pathway

Yang Liu<sup>a</sup>, Hongguang Guo<sup>a, b,\*</sup>, Yongli Zhang<sup>a</sup>, Xin Cheng<sup>a</sup>, Peng Zhou<sup>a</sup>, Jing Deng<sup>c</sup>, Jingquan Wang<sup>a</sup>, Wei Li<sup>a</sup>

<sup>a</sup> College of Architecture and Environment, Sichuan University, Chengdu 610065, China

<sup>b</sup> Department of Civil & Environmental Engineering, University of Washington, Box 352700, Seattle, WA 98195-2700, United States

<sup>c</sup> College of Civil Engineering and Architecture, Zhejiang University of Technology, Hangzhou 310014, China

\*Corresponding author. Tel: +86-028-85408889; fax: +86-028-85405534

Email: hguo@scu.edu.cn

**Abstract:** We first report the syntheses of carbon-supported Co (CS-Co) composite via a carbonization process from a saturated resin. CS-Co exhibited favorable catalysis activities in activation of peroxymonosulfate (PMS) to generate  $\cdot\text{SO}_4^-$  and  $\cdot\text{OH}$  for trimethoprim (TMP) degradation. The performance of composites were studied with respect to diverse pHs (3.0-9.0), catalyst dosages (0.05-0.5 g/L), PMS dosages (0.05-1.0 mM), TMP concentration (5-20 mg/L) and temperature (15-30°C). Water matrix concerning various levels of humic acid (HA) showed negative effect for TMP removal due to the intrinsic competition between HA. Scavenging test indicated that  $\cdot\text{SO}_4^-$  and  $\cdot\text{OH}$  were the dominant reactive radicals, and an uncomplicated method to calculate the normalized steady-state concentration of radicals in CS-Co/PMS process was established. The electron transfer concerning PMS, carbon surface and  $\text{Co}^{2+}$  was attributed as the main activation mechanism. The main intermediate products of TMP were identified by LC/MS/MS technology with four degradation pathways proposed, including hydroxylation, electron transfer mechanism, demethylation and ring-cleavage.

**Keywords:** cationic resin, carbonation, peroxymonosulfate, mechanism, degradation pathway

## 1. Introduction

Recently, sulfate radical-based advanced oxidation processes (SR-AOPs) are commonly recognized as one of the most effective ways, because of their ability to completely degrade wide variety of contaminants [1-3] **Error! Bookmark not defined.** As a dominant oxidizing species, sulfate radical ( $\cdot\text{SO}_4^-$ ) possesses an oxidation potential (2.5-3.1 V vs. normal hydrogen electrode, NHE), which is comparable or even higher than hydroxyl radicals ( $\cdot\text{OH}$ , 1.9-2.7 V).  $\cdot\text{SO}_4^-$  is extensively utilized due to its high reactivity, longer half-life period and independence of pH than  $\cdot\text{OH}$  [4, 5]. Generally,  $\cdot\text{SO}_4^-$  could be generated by the activation of peroxymonosulfate (PMS) or persulfate (PS). Various activation methods have been proposed, including heat [6], UV light [7], base [8], ultrasound [9], transition metals [10] and carbon-based catalysts [11]. Furthermore, compared with PS, PMS needs a low energy input, and displays a more efficient performance in organic contaminants degradation due to the higher oxidation potential [12].

Compared with high energy-based activation methods (UV light, thermal, etc.), the transition metal activation method showed efficient decontamination of organic contaminants, less complex in system configuration and more economical. Previous studies have demonstrated that PMS could be activated via a series of transition metals, such as Co, Mn, Fe, Cu, Ni, Ce and V, among which Co was found to be one of the most effective homogeneous catalysts [13, 14]. However, Co-based homogeneous catalysis technologies are restricted to practical applications for wastewater treatment due to its hardly separation or reuse, the possibly toxic and carcinogenic for the ecosystem and human beings, and requiring secondary treatment [15]. To overcome these drawbacks, Co-based heterogeneous catalysts, such as  $\text{Co}_3\text{O}_4$  [16], Co-OMC [17],  $\text{Fe}_x\text{Co}_{3-x}\text{O}_4$  [18],  $\text{CoFe}_2\text{O}_4$  [19], Co/AC [20], were recently investigated. These Co-based heterogeneous catalysts were reported to be efficient for activating PMS to generate  $\cdot\text{SO}_4^-$  and  $\cdot\text{OH}$ , and thus promoting effective oxidation processes of removal of organic contaminants.

Recently, carbon-based materials have been used as adsorptive support for metal

catalysts, to form carbon-supported metal composites. These composites were applied to water treatment, because metal intrinsic catalytic activity for PMS activation contribute to the degradation on contaminants [21, 22]. Recently, a novel magnetic carbon xerogels (CX/CoFe) catalyst was capable of activating persulfate for the degradation of BPA [23]. Since the cationic resin wastes are becoming a serious problem in the environment, metal-immobilized materials based on solid wastes were synthesized and applied in wastewater treatment for reuse of waste resin and solve the second pollution concern [24, 25]. However, as far as we know, none of studies has been reported on utilization of cobalt-containing waste cationic resin chars, and for the combination with PMS for contaminants removal.

In this work, cationic resin was used to fix and recycle cobalt ions in water, and carbonized through high temperature to prepare carbon-supported Co (CS-Co) composite. The structural and physicochemical properties of CS-Co samples were characterized via various techniques. The catalytic activities of CS-Co was investigated by activating PMS for trimethoprim (TMP) degradation, which is a commonly bacteriostatic antibiotic and has been detected in many natural water as a reluctant chemical, due to the high stability and large quantity in use [26, 27]. Crucial reaction parameters, such as initial pH, concentration of target, PMS and catalyst and reaction temperature, were investigated in CS-Co/PMS process. Steady-state concentration of reactive oxygen species (ROS) was calculated combined with the kinetic results. Finally, the degradation mechanism for this coupled system was demonstrated based on the scavenger experiments, with the degradation pathway of TMP proposed using LC/MS/MS. Our work provides a potential method to solve the hazardous waste problem from saturated resin with metal residual used in industrial waste water, through which a novel activation method for PMS on removing reluctant contaminants could also be expected in the aquatic environment.

## 2. Material and Methods

### 2.1 Chemical

Acidic styrene type cation exchange resin was supplied by Kelong Chemical Reagent Co. Ltd. Peroxymonosulfate ( $2\text{KHSO}_5 \cdot \text{KHSO}_4 \cdot \text{K}_2\text{SO}_4$ , PMS) and acetonitrile (HPLC grade) were purchased from Sigma-Aldrich (Shanghai, China). Trimethoprim (TMP, 99.9%) was purchased from TCI Scientific Ltd. (Shanghai, China). Cobalt nitrate ( $\text{Co}(\text{NO}_3)_2 \cdot 6\text{H}_2\text{O}$ ), tert-butanol (TBA), methanol (MA) and other reagents obtained from Kelong Chemical Reagent Co. Ltd. (Chengdu, China).

### 2.2 Preparation of CS-Co

CS-Co was synthesized via a simple carbonization method. Firstly, a certain amount of strongly acidic styrene type cation exchange resin (CAR) was sequentially soaked into 0.1 M NaOH solution and 0.1 M HCl with stirring for 3 h. The soaked products were washed with deionized water for several times until the liquid detergent pH to neutral. Then, the impregnated products was dried at  $100^\circ\text{C}$  for 12 h to form the pre-CAR. 3.0 g of pre-CAR was soaked into a solution containing 10 mM  $\text{Co}(\text{NO}_3)_2$ , and magnetically stirred for 24 h and then stood for 12 h. The residual of  $\text{Co}^{2+}$  is less-than 0.1 mM. Subsequently, the products were carbonized at  $600^\circ\text{C}$  for 2 h in a muffle furnace with  $\text{N}_2$  flow. Finally, the obtained black solid products were referred as CS-Co. The sample was also prepared by the same method without metal addition, which was referred as  $\text{CS}_0$ . The samples can be synthesized approximately 1.1-1.4 g at one time.

### 2.3 Catalyst characterization

The morphology of the samples were characterized by a Hitachi S4800 (Hitachi, Japan) scanning electron microscope (SEM) and a JEM-2010F (JEOL, Japan) transmission electron microscopy (TEM). Fourier transform infrared spectra (FT-IR) was obtained from a Bruker VERTEX 70 spectrometer. X-ray photoelectron spectroscopy (XPS) data was

obtained with an ESCALAB 250Xi (Thermo Fisher Scientific, USA) spectrometer using 300 W Al K $\alpha$  radiations. N<sub>2</sub> adsorption/desorption isotherms, pore size distribution, Brunauer-Emmett-Teller (BET) specific surface area, and pore volume were measured using a ASAP 2020 (Micromeritics, USA). The crystallographic structures of the prepared samples were characterized by X-ray diffraction (XRD) meter (D8 advance, Bruker, Germany) using monochromatized Cu K $\alpha$  ( $\lambda=1.54184$  Å, 40 kV, 40 mA). Thermal stability of CS-Co sample was investigated using thermo gravimetric analysis-differential scanning calorimetry (TGA/DSC2, METTLER TOLEDO) in air. Point of zero charge (pH<sub>PZC</sub>) of the prepared samples were determined by Mastersizer 3000 (Malvern, UK).

#### 2.4 PMS activation and TMP degradation performance

The catalytic degradation experiments were conducted in a 250 mL glass reactor on a magnetic stirrer with temperature-controlled water bath connected. Unless specifically stated, the reaction temperature was keeping at 25 °C. In a typical test, 20 mg catalyst was firstly added into the 5 mg/L TMP solution, then PMS was added into the solution at 0.5 mM. At certain intervals, 3 mL sample was periodically withdrawn and collected. The suspension sample was filtrated with glass fiber filter (Waterman, 0.45  $\mu$ m), and immediately quenched with 30  $\mu$ L methanol. The initial pH of TMP solution was about 7.00 $\pm$ 0.15. When needed, the initial pH of TMP solution was adjusted to desired value by 0.1 M H<sub>2</sub>SO<sub>4</sub> or NaOH. Triplicate experiments were performed, and the average values with the standard deviations were presented.

#### 2.5 Chemicals analysis

The concentration of TMP in the aqueous phase was quantified with a high performance liquid chromatography (HPLC) system equipped with a UV detector at a wavelength of 277 nm (Waters e2695-2489, USA). A C18 reversed phase column (150  $\times$  4.6 mm, 5  $\mu$ m particle) was used to separate organic, while mobile phase consisted of acetonitrile and water (0.1% formic acid) with a ratio of 15:85 was at a flow rate of 0.5

mL/min. The column temperature was maintained at 35 °C, and the injection volume was 20  $\mu$ L. The reaction products and intermediates were identified using LC/MS/MS, consisting of a Vanquish Flex Quaternary UHPLC coupled to a TSQ Quantum Ultra triple quadrupole mass spectrometer (Thermo Fisher Scientific, USA).

The residual of PMS concentration was determined by the iodometric method. First, 0.2 mL of the sample was diluted to 10 mL, and mixed with 0.5 g KI and 0.1 g NaHCO<sub>3</sub>. Then, the mixture was agitated vigorously shaken for 30 min, and analyzed using a UV-vis spectrophotometer (MAPADA UV-1800PC, China) at  $\lambda_{\text{max}}=354$  nm. Total organic carbon (TOC) was analyzed using a TOC analyzer (Elementar liquid TOC II, Germany). The cobalt ions concentration was determined by a PerkinElmer PinAAcle-900T atomic absorption spectrometer (AAS, USA).

### 3. Results and discussion

#### 3.1. Catalyst characterization

The textural performance of CS<sub>0</sub> and CS-Co samples were evaluated through N<sub>2</sub> adsorption/desorption isotherms (**Fig. 1**). The BET specific surface area of CS<sub>0</sub> is 9.0133 m<sup>2</sup>g<sup>-1</sup>, which is higher than CS-Co samples (3.4529 m<sup>2</sup>g<sup>-1</sup>). Otherwise, it was found that CS-Co catalyst presents a low  $V_t$  and  $V_{\text{mic}}$  than CS<sub>0</sub> sample. The pores of CS-Co and CS<sub>0</sub> samples are dominant by micropores with a diameter of around 1.2 nm. It is noted that CS-Co owns a lower pore volume and the BET specific surface area because Co occupied the micropores pore on the surface of samples. The textural properties of CS<sub>0</sub> and CS-Co samples are summarized in **Table S1**.

#### 【Fig. 1】

Moreover, the XRD patterns of the samples are illustrated in **Fig. S1**. There are no significant peaks observed in CS<sub>0</sub> samples, indicating the crystallinity CS<sub>0</sub> is low. For the pattern of CS-Co, some peaks can be observed, this is because Co and Co oxide nanoparticles dispersed on the surface of carbon spheres. Two diffraction peaks at 36.5°

and  $42.4^\circ$  corresponded to (110) and (200) crystal planes of CoO (JCPDS #43-1004), and the three peaks at  $51.1^\circ$ ,  $56.4^\circ$  and  $58.7^\circ$  are the characteristic peaks of  $\text{Co}_2\text{O}_3$  (JCPDS #02-0770). The micro-morphology of  $\text{CS}_0$  and CS-Co was investigated by SEM (**Fig. S2**). A rougher surface is observed in the image of  $\text{CS}_0$ , and some heterogeneous nanoparticles are attached to the surface. Obvious hole-structures in  $\text{CS}_0$  surface were also observed. In contrast with  $\text{CS}_0$ , Co doping had significant influence on the catalyst surface. The hole-structures disappear on the sample surface, with inconsistency nanosphere presented. The microscopic morphology of CS-Co has also been examined by TEM (**Fig. S2**), showing many cobalt oxide nanoparticles have a uniform distribution on the char layer.

The FT-IR spectra of  $\text{CS}_0$  and CS-Co materials before/after reaction are shown in **Fig. S3**. The broad absorption band at  $3430\text{ cm}^{-1}$  is associated with the O-H stretch of H-bonded  $\text{H}_2\text{O}$ , and the peaks at  $2850$  and  $2921\text{ cm}^{-1}$  are supposed to be the stretching vibration of surface -OH [28]. The absorption band at  $1610\text{ cm}^{-1}$  and  $1475\text{ cm}^{-1}$  corresponded to stretching vibration of C=O band and bending vibration of  $-\text{CH}_2$ , respectively [22, 29]. Moreover, a few peaks between  $900$  and  $1300\text{ cm}^{-1}$  are assigned to the presence of the band-type deformation oscillations of C-H and the stretching of C-O-C vibrations [22, 30].

**Fig. S4** shows the representative TGA and DTG curves of CS-Co sample, which were performed in an air atmosphere with a heating rate at  $15^\circ\text{C}/\text{min}$ . A slight weight loss occurs when the temperature was above  $478^\circ\text{C}$ . The TGA/DTG curves of the composites present a characteristic step/peak in the range from  $650$  to  $750^\circ\text{C}$ , which could be ascribed to the decomposition of carbon skeleton for the carbon coated on the cobalt oxide nanoparticles. According to the TGA profile, it can be seen that only  $11.51\text{ wt.}\%$  of CS-Co was lost, showing a good thermal stability property.

## 【Fig. 2】

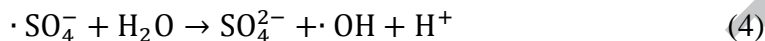
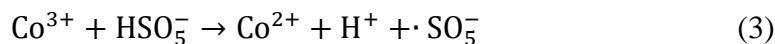
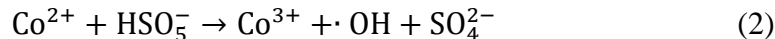
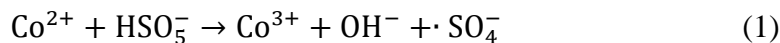
XPS analysis was performed to evaluate elemental composites and chemical states of CS-Co sample. As shown in **Fig. 2a**, the high-resolution C1s XPS spectrum is



deconvoluted into three peaks corresponded to carbon atoms in different functional groups: carbon in  $sp^2$  C-C at 284.8 eV, carbon in -CO- at 285.9 eV and carbon in -COO- at 289.5 eV [31]. According to the high resolution XPS spectra of O 1s (**Fig. 2b**), the binding energy of O1s can be deconvoluted into two peaks with 532.2 eV (O-1) and 534.0 eV (O-2), that correspond to -COOH and -OH, respectively [32]. As seen in **Fig. 2c**, the two major peaks at 781.5 eV (Co-1) and 797.6 (Co-2) eV combined with two satellite peaks (Sta.) at 785.8 eV and 802.7 eV are ascribed to Co  $2P_{3/2}$  and Co  $2P_{1/2}$ , respectively, and that corresponds to  $Co^{2+}$  (**Fig. 2c**), however, no peaks of  $Co^{3+}$  was observed [33]. These values can be attributed to cobalt cations concerned with -OH and -COO- groups, respectively, implying that the cobalt in CS-Co samples presents a high-spin  $Co^{2+}$  state [34]. Meanwhile, the peaks of  $Co^{3+}$  at 778.5 (Co-3,  $Co2P_{3/2}$ ) eV and 793.8 eV (Co-4,  $Co2P_{1/2}$ ) were observed in **Fig. 2d** for the used CS-Co [33].

### 3.2. Activation performance

The catalytic performance of CS-Co composite was further evaluated by activating peroxymonosulfate (PMS) for trimethoprim (TMP) degradation, with results illustrated in **Fig. 3a**. Single adsorption tests were carried out by only adding CS-Co into TMP solution. It can be seen that low adsorption capacities of TMP ( 5.9 %) was observed within 60 min, in accordance with the low surface areas and pore volumes in **Table S1**, and the contribution of adsorption of TMP can be neglected. The same limited removal of TMP was also demonstrated for single PMS addition. The simultaneous presence of CS-Co and PMS led to a remarkable increase of TMP degradation. As high as 96.5% removal efficiency could be achieved within 60 min, however, it is only 29.7% in  $CS_0/PMS$  system, indicating that Co element is the essential factor for the catalytic oxidation. Previous study has demonstrated that PMS could be classically activated by  $Co^{2+}$  to produce  $\cdot SO_4^-$  and  $\cdot OH$  [12] (**Eqs.1-4**). In the XPS analysis, Co element was existence as  $Co^{2+}$  in the CS-Co composite. However, in this study, only 30.5% of TMP was degraded in the  $Co^{2+}/PMS$  process, demonstrating an activation superiority for the CS-Co/PMS system.



### 【Fig. 3】

As shown in **Fig. 3b**, the residual of PMS concentration was measured under different conditions. There is no obvious PMS decomposition taking place in only PMS system, however, while quick depletion of PMS occurs with the addition of CS-Co. It indicates that the catalyst is the key role for PMS decomposition in CS-Co/PMS process. The kinetics of TMP degradation was investigated using pseudo-first-order kinetic model (Eq. 5).

$$-\ln\left(\frac{[\text{TMP}]_t}{[\text{TMP}]_0}\right) = k_{obs}t \quad (5)$$

where  $[\text{TMP}]_0$  and  $[\text{TMP}]_t$  is TMP concentration at time  $t=0$  and  $t$ , respectively and  $k_{obs}$  is the observed rate constant. The initial rate constants for TMP degradation under various systems are shown in **Fig. 3c**. A significant increase for  $k_{obs}$  was observed in the CS-Co/PMS system, reaching  $0.051 \text{ min}^{-1}$ , which is much higher than other compared systems. As shown in **Fig. 3d**, TOC measurements also confirmed the oxidative efficiency in CS-Co/PMS system, and 26.4 % of mineralization rate was achieved for TMP in 120 min reaction, suggesting that small organic compounds and inorganic carbon might generate, which will be discussed in the following section.

### 3.3 Effect of reaction parameters on TMP degradation

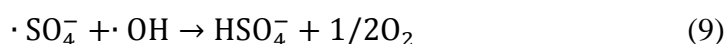
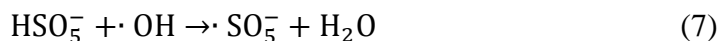
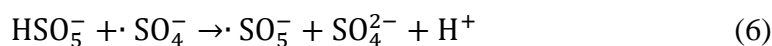
#### 3.3.1 Effect of solution pH and PMS dosage

To account for the influence of initial pH on TMP removal, the initial pH was adjusted from 3.0 to 9.0, and the results are shown in **Fig. 4**, and **Table 1**.  $k_{obs}$  for TMP was increased from  $0.010 \text{ min}^{-1}$  to  $0.051 \text{ min}^{-1}$  with the increase of pH from 3.0 to 7.0, however, limited enhancement was observed when pH value increased to 9.0. It was suggested that the pH

dependence phenomenon was mainly caused by the catalytic reaction over the catalyst surface. As shown in **Fig. S5**, the reaction solution pH was reduced to 2.8-3.5 after the stimulation, and remained stable all through the residual time. Since the  $\text{pH}_{\text{zpc}}$  of CS-Co is 5.78 (shown in **Fig. S6**), the surface of catalyst presented positive charge at pH 2.8-3.5, which was gradually decreased with pH increased. Based on the face that  $\text{TMP}^+$  and  $\text{TMP}$  fractions are the dominant species during the reaction process due to the pH-dependent dissociation of  $\text{TMP}^{++}/\text{TMP}^+/\text{TMP}$  ( $\text{pKa}_1=3.2$ ,  $\text{pKa}_2=7.1$ ) [35]. The electrostatic repulsion between catalyst and  $\text{TMP}$  ( $\text{TMP}^+$ ) was decreased with pH increased, which has an accelerative effect for  $\text{TMP}$  degradation. Therefore, the influence of initial pH on  $\text{TMP}$  removal could be attributed to the electrostatic interactions among catalyst, oxidant and the contaminant.

#### 【Fig. 4】

As summarized in **Table 1**, kinetic results show that the  $\text{TMP}$  degradation efficiency was gradually increased from 66.6% to 96.5% with the PMS concentration increased (0.1-0.5 mM). It indicates that  $\text{TMP}$  degradation can be enhanced under higher PMS concentration. Nevertheless, a lower removal efficiency was observed with PMS concentration further increasing due to the self-quenching between  $\text{HSO}_5^-$  and  $\text{ROS}$ , or  $\text{SO}_4^{\cdot-}$  and  $\cdot\text{OH}$  (**Eqs. 6-9**) [36].



#### 3.3.2 Effect of catalyst loading and initial $\text{TMP}$ concentration

As summarized in **Table 1**, at various catalyst dosages, a positive effect is clearly observed as expected, and  $k_{\text{obs}}$  increased from 0.012 to 0.100  $\text{min}^{-1}$  for catalyst dosages 0.05-0.5 g/L. The increase in catalyst loading provided more active sites for PMS activation,

thus facilitating the generation of more  $\cdot\text{SO}_4$  and  $\cdot\text{OH}$  [37]. TMP degradation efficiency was remarkably inhibited with the initial concentration of TMP increase from 5 to 20 mg/L for lack of enough  $\cdot\text{SO}_4$  and  $\cdot\text{OH}$ . In addition, a large number of generated intermediates might cause the competition effect for  $\cdot\text{SO}_4$  and  $\cdot\text{OH}$ , also the intimate contact interface between PMS and active sites of the CS-Co could be impeded at higher concentration of the contaminant [22].

### 【Table 1】

#### 3.3.3 Effect of reaction temperature

Since PMS decomposition is an endothermic reaction, the effect of temperature in this reaction system was also investigated (**Fig. 5a**). The removal of TMP had a relatively obvious change when increase the temperature from 15°C to 30°C. The removal efficiency of TMP reached 97.5% at 30°C, while only 52.5% of TMP was eliminated at 15°C, indicating that higher temperature had a beneficial stimulation in the CS-Co/PMS system. Furthermore, **Table S2** indicated that a 5 times increase was obtained for the degradation rate with the temperature increased from 15 to 30°C. The results demonstrated that higher temperature demonstrated a significant facilitation for CS-Co/PMS process to produce ROS, which could accelerate the decomposition of PMS and the movement of oxidant, intermediates, TMP molecules [38]. According to the Arrhenius equation:

$$\ln k = \ln A - \frac{E_a}{RT} \quad (10)$$

where  $E_a$  is the apparent activation energy,  $A$  denotes the pre-exponential factor,  $R$  is the gas constant (8.314 J/mol·K).  $T$  is the absolute temperature, and  $k$  is the reaction constant under different temperature. Using the  $k_{obs}$ ,  $\ln k$  was obtained and fitted into the Arrhenius equation to calculate  $E_a$  and  $A$  for TMP degradation in this heterogeneous system. **Fig. 5b** demonstrates the relationship between  $k_{obs}$  and temperature. The  $E_a$  of TMP degradation was 96.7 kJ/mol, which is obviously lower than that reported in the previous study for

thermo-activated persulfate (177.8 kJ/mol) [39].

### 3.3.4 Effect of organic matrix

In order to elucidate the characteristics in CS-Co/PMS system, the experiments concerning of various concentrations of HA (5 ppm to 20 ppm) and water quality were conducted. As shown in **Fig. 5c**, TMP degradation efficiency decreased from 96.5% to 46.9% with HA concentration increasing (0 ppm to 20 ppm). The  $k_{obs}$  in presence of 5, 10 and 20 ppm HA was found to be 0.027, 0.018 and 0.011  $\text{min}^{-1}$  respectively compared to 0.051  $\text{min}^{-1}$  in the control test. The retardation of TMP degradation could be attribute to the competition reaction between HA and TMP for  $\cdot\text{SO}_4^-$  and  $\cdot\text{OH}$  [23]. Moreover, TMP degradation efficiency was also adequately receded in river water (RW) and tap water (TW) (**Fig. 5d**). The physicochemical parameters of RW are presented in **Table S3**. Obviously, CS-Co/PMS process was able to remove 96.5%, 89.4% and 66.0% of TMP from UPW, TW and RW, respectively. The degradation efficiency of TMP in various water matrices followed: UPW ( $k_{obs}=0.051 \text{ min}^{-1}$ )>TW ( $k_{obs}=0.045 \text{ min}^{-1}$ )>RW ( $k_{obs}=0.028 \text{ min}^{-1}$ ). Compared to UPW, sound inhibition was observed in TW and RW, owing to the quenching effect. Despite that, the degradation efficiency of TMP is acceptable in CS-Co/PMS/RW process.

### 【Fig. 5】

## 3.4 Catalysis mechanism discussion

### 3.4.1 Determination of principal reaction radicals

Previous have demonstrated that  $\cdot\text{SO}_5^-$ ,  $\cdot\text{SO}_4^-$  and  $\cdot\text{OH}$  were the main ROS in SR-AOP process [2]. To confirm the major ROS formed in CS-Co/PMS process, and to evaluate each one contribution for TMP removal, quenching studies with different radical scavengers were performed. Methanol (MA) and tert-butanol (TBA) were selected as probe chemicals, because MA is capable for quenching  $\cdot\text{SO}_4^-$  as well as  $\cdot\text{OH}$  for the high

reactivity towards the both radicals, but TBA is a particular scavenger for  $\cdot\text{OH}$  [40]. **Fig. 6a** shows the TMP degradation efficiency in the presence of both quenching reagents. About 96.1% TMP was degraded when no quenching agents were added. However, a significant inhibition on the degradation of TMP could be observed in the presence of TBA and MA. More specifically, 68.2% of TMP degradation efficiencies were achieved when 50 mM TBA was presented, while only 9.5% of TMP degradation was attained in presence of the same concentration of methanol. Therefore, both  $\cdot\text{SO}_4^-$  and  $\cdot\text{OH}$  are the dominant radicals in the CS-Co/PMS process.

### 【Fig. 6】

A large number of Co-based heterogeneous catalyst for PMS activation have been studied via various preparation methods for contaminants removal [41, 42]. The catalysis activation process is acceptable that formed  $\text{CoOH}^+$  and  $\text{Co}^{2+}$  are regarded as the most effective species for PMS activation on the Co-catalyst surface [43, 44]. Correspondingly, decreasing PMS concentration could be expected in the Co-based/PMS system. **Fig. 6b** shows the PMS concentration changing under diverse quenching experiments. This results are consistent with previous reports concerning PMS activation [41, 45].

#### 3.4.2 Estimation of steady-state $\cdot\text{SO}_4^-$ and $\cdot\text{OH}$ concentration

According to the analysis above, we speculated that  $\cdot\text{SO}_4^-$  and  $\cdot\text{OH}$  are major ROS dominating TMP degradation. As analyzed by BET (**Fig. 1**) and XPS (**Fig. 2**), carbon-based material not only provides a large surface area with unique physicochemical properties, but also have lots of active groups to ensure the favorable immobilization and excellent dispersion of ROS, such as  $-\text{CO}-$ , which was reported as a activator for PMS [46]. Besides, carbon-based surface also provide multitudinous electron transfer channels, leading to a higher electron transfer rate between catalyst surface and PMS [2]. For instance, Zhou et al. reported a carbon microsphere supported by cobalt catalysts, which showed a superior catalytic performance by activation of PMS for phenol degradation [47].

On the basis of the above results, a feasible mechanism in the CS-Co/PMS process is proposed in **Fig. 7**.

**【Fig. 7】**

Different concentration of MA and TBA for TMP removal in the CS-Co/PMS process were also conducted (**Fig. S7**). It is seen that the inhibition was not furtherly enhanced when the concentration of MA and TBA increased to 50 mM. Therefore, it is possible to evaluate the radical contribution percentage *via* a facile method. The percentage of the sulfate radicals ( $\cdot\text{SO}_4^-$ ) reacted with TMP was calculated using the following this equation:

$$r_{\cdot\text{SO}_4^-} = \left( \frac{k_{\text{obs}}(\cdot\text{SO}_4^-)}{k_{\text{obs}}(\cdot\text{SO}_4^- + \cdot\text{OH})} \right) \times 100\% \quad (11)$$

where  $k_{\text{obs}}$  is the pseudo-first-order rate constant. According to the previous study, we can suppose that the deviations observed for TMP removal (i.e. 40%) should correspond to the contribution of  $\cdot\text{SO}_4^-$ , when different radical scavengers were used separately in CS-Co/PMS process [48]. Thus, the relative contribution of  $\cdot\text{OH}$  to the degradation of TMP is estimated as 60%. It is feasible to estimate the normalized steady-state concentration of  $\cdot\text{SO}_4^-$  ( $[\cdot\text{SO}_4^-]_{\text{N}}$ ) and  $\cdot\text{OH}$  ( $[\cdot\text{OH}]_{\text{N}}$ ) using the aqueous concentration of chemicals and the reactivity of radicals with TMP ( $k_{\text{TMP}/\cdot\text{SO}_4^-} = 7.71 \pm 0.29 \times 10^9 \text{ M}^{-1}\text{s}^{-1}$ ;  $k_{\text{TMP}/\cdot\text{OH}} = 8.34 \pm 0.25 \times 10^9 \text{ M}^{-1}\text{s}^{-1}$ ) [39]. Based on the degradation rate of TMP with respect to the steady-state concentration of  $\cdot\text{SO}_4^-$  [ $\cdot\text{SO}_4^-$ ] and  $\cdot\text{OH}$  [ $\cdot\text{OH}$ ], the pseudo first-order assumption can be obtained as follows [49]:

$$-\frac{d_{[\text{TMP}]}}{dt} = k_{\text{TBA}/\cdot\text{SO}_4^-}[\text{TMP}][\cdot\text{SO}_4^-] + k_{\text{TMP}/\cdot\text{OH}}[\text{TMP}][\cdot\text{OH}] \quad (12)$$

Taking into consideration that the contribution of  $\cdot\text{OH}$  for TMP degradation was 60%, which is 1.5 times for the  $\cdot\text{SO}_4^-$  contribution, the kinetic expression becomes:

$$-\frac{d_{[\text{TMP}]}}{dt} = k_{\text{TMP}/\cdot\text{SO}_4^-}[\text{TMP}][\cdot\text{SO}_4^-] + 1.5k_{\text{TMP}/\cdot\text{SO}_4^-}[\text{TMP}][\cdot\text{SO}_4^-] \quad (13)$$

$$-\frac{d_{[\text{TMP}]}}{dt} = 2.5k_{\text{TMP}/\cdot\text{SO}_4^-}[\text{TMP}][\cdot\text{SO}_4^-] = k_{\text{obs}}[\text{TMP}] \quad (14)$$

Thus, the  $[\cdot\text{SO}_4^-]$  and the normalizing  $\cdot\text{SO}_4^-$   $[\cdot\text{SO}_4^-]_{\text{N}}$  can be obtained as follows:

$$[\cdot \text{SO}_4^-] = \frac{k_{\text{obs}}}{2.5k_{\text{TMP}/\cdot\text{SO}_4^-}} \quad (15)$$

$$[\cdot \text{SO}_4^-]_{\text{N}} = \frac{k_{\text{obs}}}{2.5\text{LD}k_{\text{TMP}/\cdot\text{SO}_4^-}} \quad (16)$$

Using the same calculation process, the  $[\cdot\text{OH}]$  and the normalizing the  $[\cdot\text{OH}]_{\text{N}}$  can be obtained as follows:

$$[\cdot \text{OH}] = \frac{k_{\text{obs}}}{1.67k_{\text{TMP}/\cdot\text{OH}}} \quad (17)$$

$$[\cdot \text{OH}]_{\text{N}} = \frac{k_{\text{obs}}}{1.67\text{LD}k_{\text{TMP}/\cdot\text{OH}}} \quad (18)$$

where D is the dosage of catalyst, and L is the concentration of PMS. Ultimately, the calculated  $[\cdot\text{SO}_4^-]_{\text{N}}$  and  $[\cdot\text{OH}]_{\text{N}}$  are  $1.24 \times 10^{-12} \text{ M L}^2 \text{ g}^{-1} \text{ mol}^{-1}$  and  $1.72 \times 10^{-12} \text{ M L}^2 \text{ g}^{-1} \text{ mol}^{-1}$  in CS-Co/PMS system.

### 3.5 Degradation byproducts and pathways of TMP

To elucidate the intermediates formation of TMP degradation in CS-Co/PMS process, the main products and the intermediates in the reaction were analyzed using LC/MS/MS. According to the MS<sup>2</sup> spectra results (Fig. S8-S9), ten compounds were identified in this work and summarized in Table 2. TP-1/2/3 (M/Z 307), TP-4 (M/Z 305) and TP-6/7 (M/Z 325) are the main products, which were also found in previous studies [39, 50]. Based on the identification of the intermediates and previous studies [26, 51], the TMP degradation mechanism were proposed in Fig. 8, with four pathways exhibited: hydroxylation, electron transfer mechanism, demethylation and related cleavage. The pyrimidine ring of TMP, was firstly attacked by  $\cdot\text{SO}_4^-$  via electron transfer mechanism, leading to the formation of a carbon-centered radical accompanied with the hydroxylation, demethylation and cleavage [52, 53]. In our study, three separate primary products TP-1, TP-2 and TP-3 were observed through electron transfer mechanism of  $\cdot\text{SO}_4^-$ , and hydroxylation of  $\cdot\text{OH}$ . The subsequent hydroxylation or demethylation resulted in the formation of intermediates TP-6 and TP-7. Product TP-4 was generated from the intermediate TP-1 via electron transfer mechanism and hydroxylation. In addition, TP-5 (M/Z, 279), an intermediate compound demonstrated



the simultaneous hydroxylation and cleavage. Finally, the products of TP-8 (M/Z, 111), TP-9 (M/Z, 171) and TP-10 (M/Z, 197) was believed to be derived from the cleavage.

### 【Table 2】

### 【Fig. 8】

## 4. Conclusions

A novel composite CS-Co was successfully fabricated via a facile carbonization method, and a highly efficient activation for PMS was observed on TMP degradation. Kinetic results revealed that neutral pH shows a preferable effect on the removal performance and enhanced  $k_{obs}$  was obtained with the increase of PMS dosage, catalyst loading and reaction temperature. Due to the quenching effect of HA, the degradation efficiency of TMP in various water matrices followed: UPW >TW >RW. The sound reusable was observed for CS-Co composites. Based on the scavenging results,  $\cdot\text{SO}_4$  and  $\cdot\text{OH}$  were confirmed as the main radical throughout the activation, with the normalized steady-state concentration calculated as  $1.24 \times 10^{-12} \text{ ML}^2\text{g}^{-1}\text{mol}^{-1}$  and  $1.72 \times 10^{-12} \text{ ML}^2\text{g}^{-1}\text{mol}^{-1}$ , respectively. Ten intermediates were identified in the four-pathway degradation of TMP, concerning hydroxylation, electron transfer mechanism, demethylation and cleavage.

## Acknowledgements

The authors would like to thank the National Natural Science Foundation of China (NO. 51508354, 51878422), and Science and Technology Projects of Sichuan Province (2018 HH0104) for the financial support.

## References

- [1] S. Waclawek, H.V. Lutze, K. Grübel, V.V.T. Padil, M. Černík, D.D. Dionysiou, Chemistry of persulfates in water and wastewater treatment: A review, Chem Eng J 330 (2017) 44-62.
- [2] F. Ghanbari, M. Moradi, Application of peroxymonosulfate and its activation methods for degradation of environmental organic pollutants: Review, Chem Eng J 310 (2017) 41-62.

- [3] W. Tian, H. Zhang, Z. Qian, T. Ouyang, H. Sun, J. Qin, M.O. Tadé, S. Wang, Bread-making synthesis of hierarchically Co@C nanoarchitecture in heteroatom doped porous carbons for oxidative degradation of emerging contaminants, *Appl Catal B-Environ* 225 (2018) 76-83.
- [4] Z.Z. Liu, S.J. Yang, Y.N. Yuan, J. Xu, Y.F. Zhu, J.J. Li, F. Wu, A novel heterogeneous system for sulfate radical generation through sulfite activation on a  $\text{CoFe}_2\text{O}_4$  nanocatalyst surface, *J Hazard Mater* 324 (2017) 583-592.
- [5] T. Zhou, X. Zou, J. Mao, X. Wu, Decomposition of sulfadiazine in a sonochemical  $\text{Fe}^0$ -catalyzed persulfate system: Parameters optimizing and interferences of wastewater matrix, *Appl Catal B-Environ* 185 (2016) 31-41.
- [6] Q. Wang, X. Lu, Y. Cao, J. Ma, J. Jiang, X. Bai, T. Hu, Degradation of Bisphenol S by heat activated persulfate: Kinetics study, transformation pathways and influences of co-existing chemicals, *Chem Eng J* 328 (2017) 236-245.
- [7] H.G. Guo, T.L. Ke, N.Y. Gao, Y. Liu, X. Cheng, Enhanced degradation of aqueous norfloxacin and enrofloxacin by UV-activated persulfate: Kinetics, pathways and deactivation, *Chem Eng J* 316 (2017) 471-480.
- [8] O.S. Furman, A.L. Teel, R.J. Watts, Mechanism of Base Activation of Persulfate, *Environ Sci Technol* 44 (2010) 6423-6428.
- [9] S. Chakma, S. Praneeth, V.S. Moholkar, Mechanistic investigations in sono-hybrid (ultrasound/ $\text{Fe}^{2+}$ /UVC) techniques of persulfate activation for degradation of Azorubine, *Ultrason Sonochem* 38 (2017) 652-663.
- [10] X. Duan, C. Su, J. Miao, Y. Zhong, Z. Shao, S. Wang, H. Sun, Insights into perovskite-catalyzed peroxymonosulfate activation: Maneuverable cobalt sites for promoted evolution of sulfate radicals, *Appl Catal B-Environ* 220 (2018) 626-634.
- [11] Y.C. Lee, S.L. Lo, J. Kuo, C.P. Huang, Promoted degradation of perfluorooctanoic acid by persulfate when adding activated carbon, *J Hazard Mater* 261 (2013) 463-469.
- [12] P. Hu, M. Long, Cobalt-catalyzed sulfate radical-based advanced oxidation: A review on heterogeneous catalysts and applications, *Appl Catal B-Environ* 181 (2016) 103-117.
- [13] G.P. Anipsitakis, D.D. Dionysiou, Radical generation by the interaction of transition metals with common oxidants, *Environ Sci Technol* 38 (2004) 3705-3712.
- [14] Y.J. Yao, H. Chen, C. Lian, F.Y. Wei, D.W. Zhang, G.D. Wu, B.J. Chen, S.B. Wang, Fe, Co, Ni nanocrystals encapsulated in nitrogen-doped carbon nanotubes as Fenton-like catalysts for organic pollutant removal, *J Hazard Mater* 314 (2016) 129-139.
- [15] W.D. Oh, Z.L. Dong, T.T. Lim, Generation of sulfate radical through heterogeneous catalysis for organic contaminants removal: Current development, challenges and prospects, *Appl Catal B-Environ* 194 (2016) 169-201.
- [16] X.Y. Chen, J.W. Chen, X.L. Qiao, D.G. Wang, X.Y. Cai, Performance of nano- $\text{Co}_3\text{O}_4$ /peroxymonosulfate system: Kinetics and mechanism study using Acid Orange 7 as a model compound, *Appl Catal B-Environ* 80 (2008) 116-121.
- [17] Y. Wang, D. Cao, X. Zhao, Heterogeneous degradation of refractory pollutants by peroxymonosulfate activated by CoOx-doped ordered mesoporous carbon, *Chem Eng J* 328 (2017) 1112-1121.
- [18] Z.T. Hu, Z. Chen, R. Goei, W. Wu, T.T. Lim, Magnetically recyclable Bi/Fe-based hierarchical nanostructures via self-assembly for environmental decontamination, *Nanoscale* 8 (2016) 12736-12746.

- [19] J. Deng, Y.S. Shao, N.Y. Gao, C.Q. Tan, S.Q. Zhou, X.H. Hu,  $\text{CoFe}_2\text{O}_4$  magnetic nanoparticles as a highly active heterogeneous catalyst of oxone for the degradation of diclofenac in water, *J Hazard Mater* 262 (2013) 836-844.
- [20] P.R. Shukla, S.B. Wang, H.Q. Sun, H.M. Ang, M. Tade, Activated carbon supported cobalt catalysts for advanced oxidation of organic contaminants in aqueous solution, *Appl Catal B-Environ* 100 (2010) 529-534.
- [21] J. Du, J. Bao, Y. Liu, H. Ling, H. Zheng, S.H. Kim, D.D. Dionysiou, Efficient activation of peroxymonosulfate by magnetic Mn-MGO for degradation of bisphenol A, *J Hazard Mater* 320 (2016) 150-159.
- [22] P. Hu, M. Long, X. Bai, C. Wang, C. Cai, J. Fu, B. Zhou, Y. Zhou, Monolithic cobalt-doped carbon aerogel for efficient catalytic activation of peroxymonosulfate in water, *J Hazard Mater* 332 (2017) 195-204.
- [23] A. Outsouk, Z. Frontistis, R.S. Ribeiro, M. Antonopoulou, I.K. Konstantinou, A.M.T. Silva, J.L. Faria, H.T. Gomes, D. Mantzavinos, Activation of sodium persulfate by magnetic carbon xerogels (CX/CoFe) for the oxidation of bisphenol A: Process variables effects, matrix effects and reaction pathways, *Water Res* 124 (2017) 97-107.
- [24] Q. Shi, A. Li, Z. Qing, Y. Li, Oxidative degradation of Orange G by persulfate activated with iron-immobilized resin chars, *J Ind Eng Chem* 25 (2015) 308-313.
- [25] Z. Wan, L.J. Xu, J.L. Wang, Treatment of spent radioactive anionic exchange resins using Fenton-like oxidation process, *Chem Eng J* 284 (2016) 733-740.
- [26] G.A.K. Anquandah, V.K. Sharma, D.A. Knight, S.R. Batchu, P.R. Gardinali, Oxidation of Trimethoprim by Ferrate(VI): Kinetics, Products, and Antibacterial Activity, *Environ Sci Technol* 45 (2011) 10575-10581.
- [27] Z. Wu, J. Fang, Y. Xiang, C. Shang, X. Li, F. Meng, X. Yang, Roles of reactive chlorine species in trimethoprim degradation in the UV/chlorine process: Kinetics and transformation pathways, *Water Res* 104 (2016) 272-282.
- [28] T. Zhang, H. Zhu, J.-P. Croué, Production of Sulfate Radical from Peroxymonosulfate Induced by a Magnetically Separable  $\text{CuFe}_2\text{O}_4$  Spinel in Water: Efficiency, Stability, and Mechanism, *Environ Sci Technol* 47 (2013) 2784-2791.
- [29] S. Anjum, R. Tufail, K. Rashid, R. Zia, S. Riaz, Effect of cobalt doping on crystallinity, stability, magnetic and optical properties of magnetic iron oxide nano-particles, *J Magn Magn Mater* 432 (2017) 198-207.
- [30] Y. Leng, W. Guo, X. Shi, Y. Li, L. Xing, Polyhydroquinone-Coated  $\text{Fe}_3\text{O}_4$  Nanocatalyst for Degradation of Rhodamine B based on Sulfate Radicals, *Ind Eng Chem Res* 52 (2013) 13607-13612.
- [31] J. Dou, S. Yin, J.Y. Chong, B. Zhang, J. Han, Y. Huang, R. Xu, Carbon spheres anchored  $\text{Co}_3\text{O}_4$  nanoclusters as an efficient catalyst for dye degradation, *Appl Catal A- Gen* 513 (2016) 106-115.
- [32] Y.W. Gao, Z.Y. Zhang, S.M. Li, J. Liu, L.Y. Yao, Y.X. Li, H. Zhang, Insights into the mechanism of heterogeneous activation of persulfate with a clay/iron-based catalyst under visible LED light irradiation, *Appl Catal B-Environ* 185 (2016) 22-30.
- [33] V.H. Nguyen, J.-J. Shim, In situ growth of hierarchical mesoporous  $\text{NiCo}_2\text{S}_4@\text{MnO}_2$  arrays on nickel foam for high-performance supercapacitors, *Electrochim Acta* 166 (2015) 302-309.
- [34] C. Gong, F. Chen, Q. Yang, K. Luo, F. Yao, S. Wang, X. Wang, J. Wu, X. Li, D. Wang, G. Zeng, Heterogeneous activation of peroxymonosulfate by Fe-Co layered doubled hydroxide for efficient catalytic degradation of Rhoadmine B, *Chem Eng J* 321 (2017) 222-232.

- [35] R. Zhang, P. Sun, T.H. Boyer, L. Zhao, C.H. Huang, Degradation of pharmaceuticals and metabolite in synthetic human urine by UV, UV/H<sub>2</sub>O<sub>2</sub>, and UV/PDS, *Environ Sci Technol* 49 (2015) 3056-3066.
- [36] M. Nie, C. Yan, M. Li, X. Wang, W. Bi, W. Dong, Degradation of chloramphenicol by persulfate activated by Fe<sup>2+</sup> and zerovalent iron, *Chem Eng J* 279 (2015) 507-515.
- [37] E. Saputra, S. Muhammad, H.Q. Sun, H.M. Ang, M.O. Tade, S.B. Wang, Manganese oxides at different oxidation states for heterogeneous activation of peroxymonosulfate for phenol degradation in aqueous solutions, *Appl Catal B-Environ* 142 (2013) 729-735.
- [38] D. Chen, X. Ma, J. Zhou, X. Chen, G. Qian, Sulfate radical-induced degradation of Acid Orange 7 by a new magnetic composite catalyzed peroxymonosulfate oxidation process, *J Hazard Mater* 279 (2014) 476-484.
- [39] Y.F. Ji, W.P. Xie, Y. Fan, Y.Y. Shi, D.Y. Kong, J.H. Lu, Degradation of trimethoprim by thermo-activated persulfate oxidation: Reaction kinetics and transformation mechanisms, *Chem Eng J* 286 (2016) 16-24.
- [40] Y. Liu, H. Guo, Y. Zhang, W. Tang, X. Cheng, H. Liu, Activation of peroxymonosulfate by BiVO<sub>4</sub> under visible light for degradation of Rhodamine B, *Chem Phys Lett* 653 (2016) 101-107.
- [41] C. Cai, H. Zhang, X. Zhong, L.W. Hou, Ultrasound enhanced heterogeneous activation of peroxymonosulfate by a bimetallic Fe-Co/SBA-15 catalyst for the degradation of Orange II in water, *J Hazard Mater* 283 (2015) 70-79.
- [42] Q. Han, S.Y. Yang, X. Yang, X.T. Shao, R. Niu, L.L. Wang, Cobalt Catalyzed Peroxymonosulfate Oxidation : A Review of Mechanisms and Applications on Degrading Organic Pollutants in Water, *Prog Chem* 24 (2012) 144-156.
- [43] F.J. Rivas, O. Gimeno, T. Borallho, Aqueous pharmaceutical compounds removal by potassium monopersulfate. Uncatalyzed and catalyzed semicontinuous experiments, *Chem Eng J* 192 (2012) 326-333.
- [44] P.H. Shi, X.F. Dai, H.G. Zheng, D.X. Li, W.F. Yao, C.Y. Hu, Synergistic catalysis of Co<sub>3</sub>O<sub>4</sub> and graphene oxide on Co<sub>3</sub>O<sub>4</sub>/GO catalysts for degradation of Orange II in water by advanced oxidation technology based on sulfate radicals, *Chem Eng J* 240 (2014) 264-270.
- [45] Y.M. Ren, L.Q. Lin, J. Ma, J. Yang, J. Feng, Z.J. Fan, Sulfate radicals induced from peroxymonosulfate by magnetic ferrosphenel MFe<sub>2</sub>O<sub>4</sub> (M = Co, Cu, Mn, and Zn) as heterogeneous catalysts in the water, *Appl Catal B-Environ* 165 (2015) 572-578.
- [46] Y.X. Wang, Z.M. Ao, H.Q. Sun, X.G. Duan, S.B. Wang, Activation of peroxymonosulfate by carbonaceous oxygen groups: experimental and density functional theory calculations, *Appl Catal B-Environ* 198 (2016) 295-302.
- [47] G.L. Zhou, L. Zhou, H.Q. Sun, H.M. Ang, M.O. Tade, S.B. Wang, Carbon microspheres supported cobalt catalysts for phenol oxidation with peroxymonosulfate, *Chem Eng Res Des* 101 (2015) 15-21.
- [48] M. Kamagate, A.A. Assadi, T. Kone, L. Coulibaly, K. Hanna, Activation of persulfate by irradiated laterite for removal of fluoroquinolones in multi-component systems, *J Hazard Mater* 346 (2018) 159-166.
- [49] W.D. Oh, Z.L. Dong, T.T. Lim, Hierarchically-structured Co-CuBi<sub>2</sub>O<sub>4</sub> and Cu-CuBi<sub>2</sub>O<sub>4</sub> for sulfanilamide removal via peroxymonosulfate activation, *Catal Today* 280 (2017) 2-7.
- [50] R. Zhang, Y. Yang, C.H. Huang, N. Li, H. Liu, L. Zhao, P. Sun, UV/H<sub>2</sub>O<sub>2</sub> and UV/PDS Treatment of Trimethoprim and Sulfamethoxazole in Synthetic Human Urine: Transformation Products and Toxicity, *Environ Sci Technol* 50 (2016) 2573-2583.
- [51] I. Michael, E. Hapeshi, V. Osorio, S. Perez, M. Petrovic, A. Zapata, S. Malato, D. Barcelo, D. Fatta-

Kassinis, Solar photocatalytic treatment of trimethoprim in four environmental matrices at a pilot scale: Transformation products and ecotoxicity evaluation, *Sci Total Environ* 430 (2012) 167-173.

[52] Z. Zhang, Q. Yang, J. Wang, Degradation of trimethoprim by gamma irradiation in the presence of persulfate, *Radiat Phys Chem* 127 (2016) 85-91.

[53] S.Z. Wang, J.L. Wang, Trimethoprim degradation by Fenton and Fe(II)-activated persulfate processes, *Chemosphere* 191 (2018) 97-105.

ACCEPTED MANUSCRIPT

## Tables

### Table captions

**【Table 1】** Fitting parameters of pseudo-first-order kinetics model under various conditions on degradation of TMP by PMS activation using CS-Co composite.

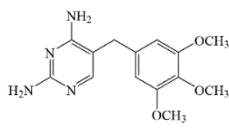
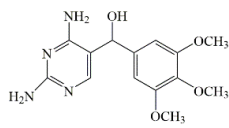
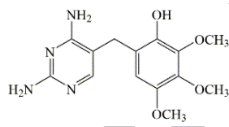
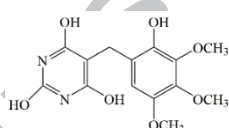
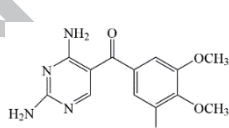
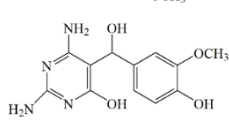
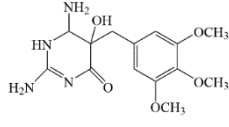
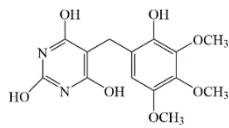
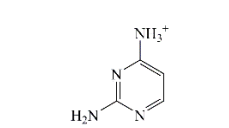
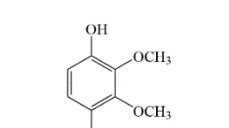
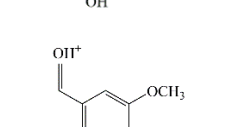
**【Table 2】** The intermediate compounds detected in CS-Co/PMS process.

ACCEPTED MANUSCRIPT

**Table 1**

pH	Initial concentration for TMP /mg·L <sup>-1</sup>	PMS dosage /mM	Catalyst /g·L <sup>-1</sup>	$k_{\text{obs}}/\text{min}^{-1}$	$t_{1/2}/\text{min}$	R <sup>2</sup>
3.0	5	0.5	0.1	0.010±0.001	70.44	0.993
5.0	5	0.5	0.1	0.037±0.004	18.96	0.924
7.0	5	0.5	0.1	0.051±0.006	13.67	0.928
9.0	5	0.5	0.1	0.048±0.004	14.44	0.967
7.0	5	0.05	0.1	0.028±0.002	24.93	0.992
7.0	5	0.1	0.1	0.030±0.001	22.88	0.986
7.0	5	0.2	0.1	0.036±0.002	19.06	0.987
7.0	5	0.25	0.1	0.040±0.002	17.33	0.973
7.0	5	0.5	0.1	0.051±0.006	13.67	0.934
7.0	5	1.0	0.1	0.045±0.005	15.48	0.928
7.0	5	0.5	0.05	0.012±0.001	58.74	0.959
7.0	5	0.5	0.1	0.051±0.006	13.67	0.934
7.0	5	0.5	0.2	0.060±0.004	11.51	0.981
7.0	5	0.5	0.3	0.069±0.003	10.10	0.990
7.0	5	0.5	0.5	0.100±0.003	6.93	0.992
7.0	5	0.5	0.1	0.051±0.006	13.67	0.932
7.0	10	0.5	0.1	0.012±0.001	59.70	0.986
7.0	15	0.5	0.1	0.008±0.002	84.53	0.988
7.0	20	0.5	0.1	0.007±0.001	103.45	0.969

Table 2

Compound	M/Z	Intermediate
TMP	291	
TP-1	307	
TP-2	307	
TP-3	307	
TP-4	305	
TP-5	279	
TP-6	325	
TP-7	325	
TP-8	111	
TP-9	171	
TP-10	197	



ACCEPTED MANUSCRIPT

## Figures

### Figure captions

**【Fig. 1】** N<sub>2</sub> adsorption/desorption isotherms of samples: (a) CS<sub>0</sub>; (b) CS-Co.

**【Fig. 2】** The XPS spectra of CS-Co: (a) high-resolution C1s; (b) high-resolution O1s; high-resolution Co2p<sub>3/2</sub> and Co2p<sub>1/2</sub>, fresh (c) and used CS-Co (d).

**【Fig. 3】** Removal performance of TMP in various reaction systems with indicators monitoring: (a) C<sub>t</sub>/C<sub>0</sub>; (b) PMS concentration; (c) *k*<sub>obs</sub>; (d) TOC in CS-Co/PMS system ([TMP]=5 mg/L, [PMS]=0.50 mM, [catalyst]=0.1 g/L, [Co<sup>2+</sup>]=0.01 mM, T=25 °C, initial pH).

**【Fig. 4】** Effect of initial pH on TMP degradation. ([TMP]=5 mg/L, [PMS]=0.50 mM [catalyst]=0.1 g/L, T=25 °C, initial pH or adjusted pH).

**【Fig. 5】** (a) Influence of reaction temperatures on the removal of TMP; (b) Estimation of activation energy; (c) Effect of HA; (d) Effect of actual water matrix ([TMP]=5 mg/L, [PMS]=0.50 mM, [catalyst]=0.1 g/L, initial pH).

**【Fig. 6】** (a) Competitive radical quenching tests; (b) PMS concentration changing ([TMP]=5 mg/L, [PMS]=0.50 mM, [MA]= [TBA]=50 mM, [catalyst]=0.1 g/L, T=25 °C, initial pH).

**【Fig. 7】** The proposed mechanism for TMP degradation in CS-Co/PMS process.

**【Fig. 8】** Degradation pathways of TMP by CS-Co/PMS process.

Fig. 1

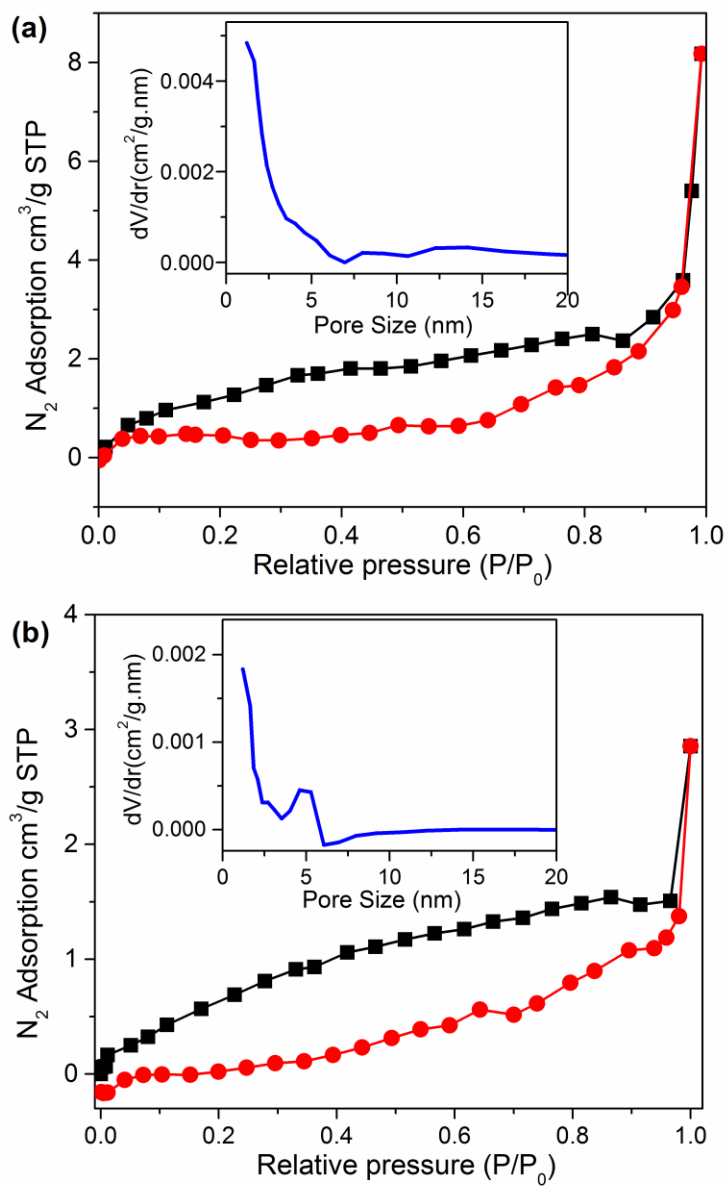


Fig. 2

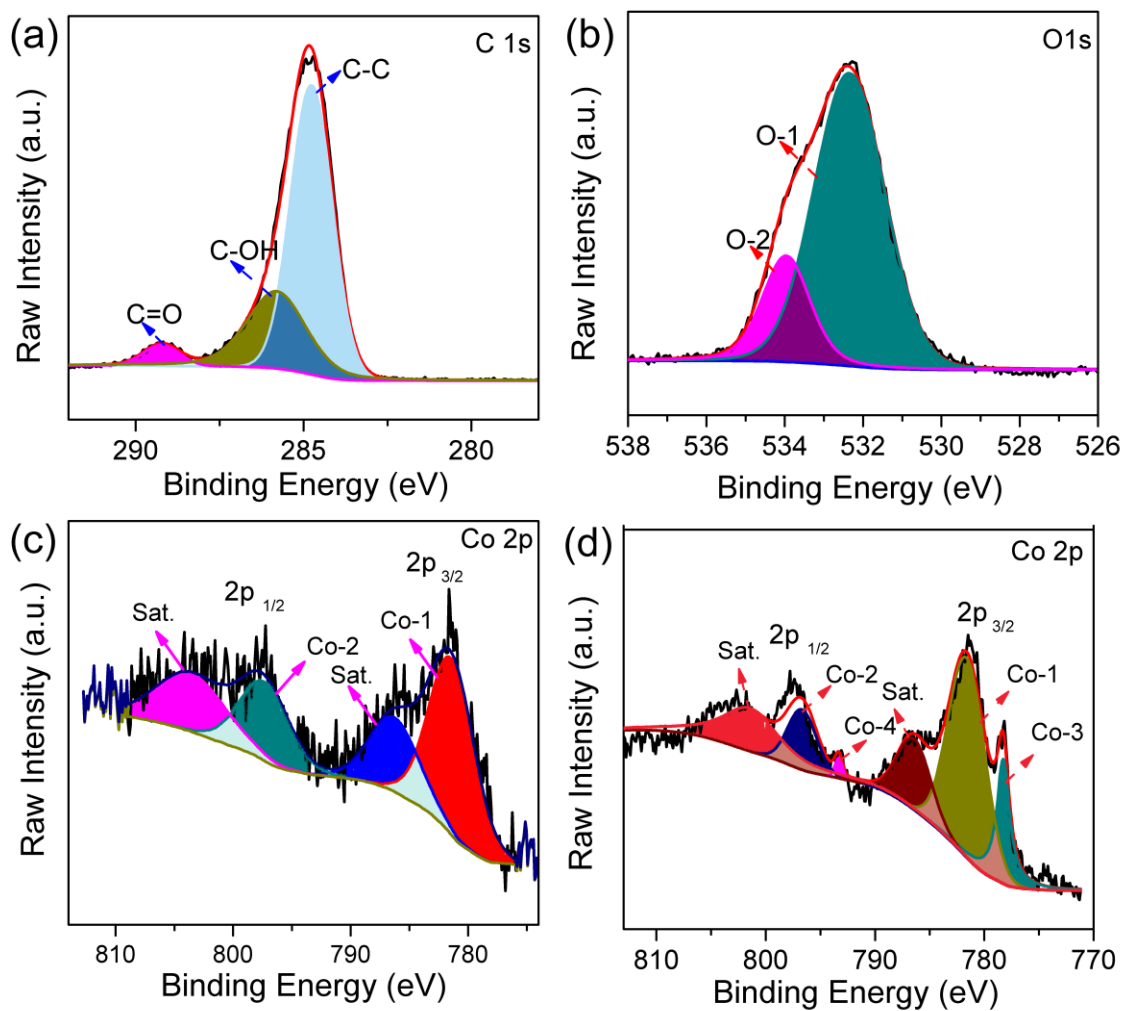


Fig. 3

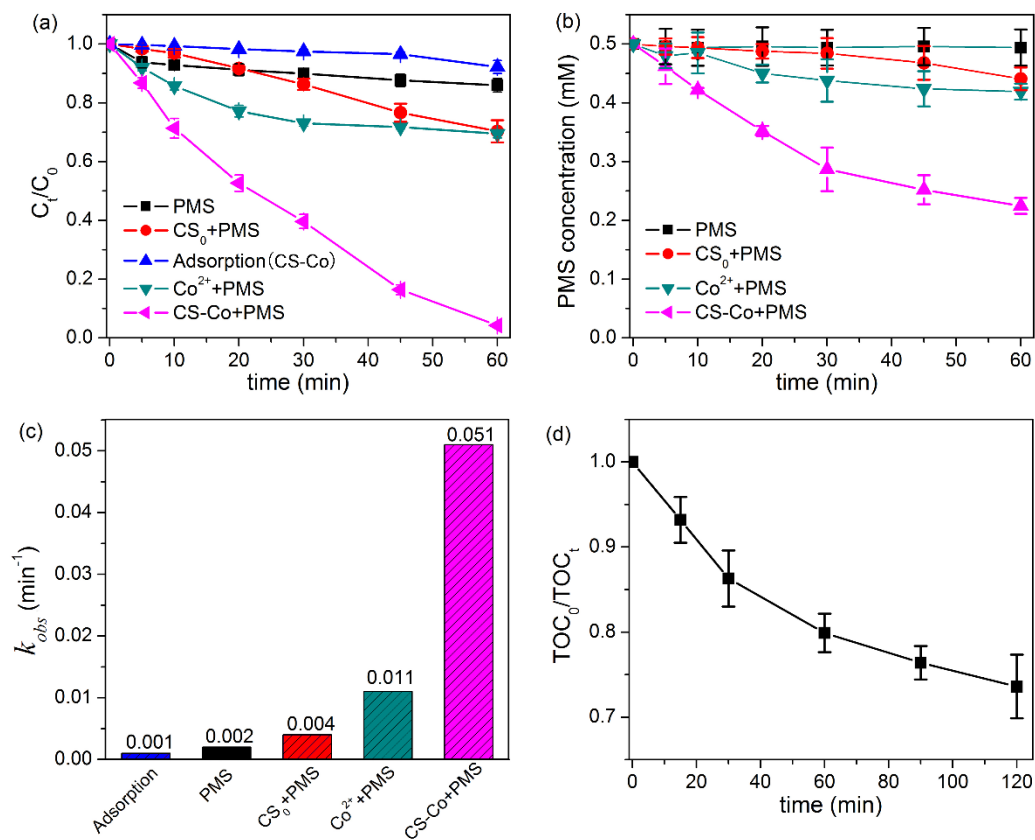


Fig. 4

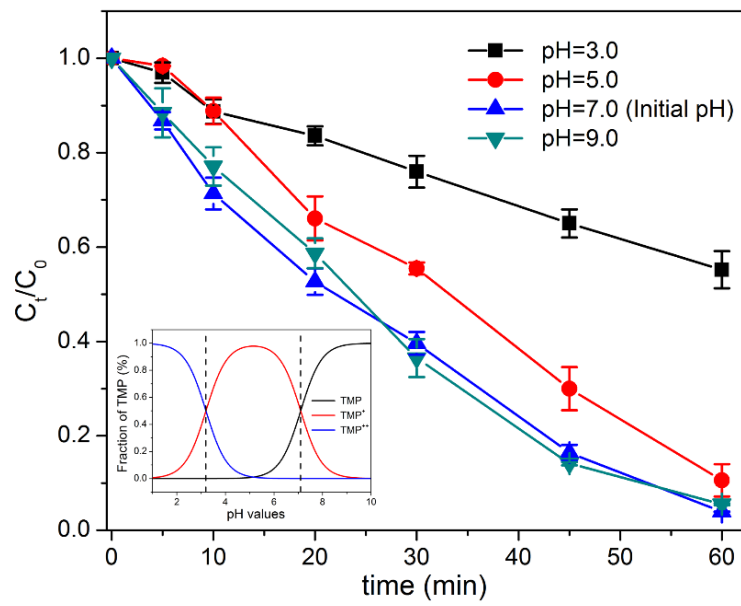


Fig. 5

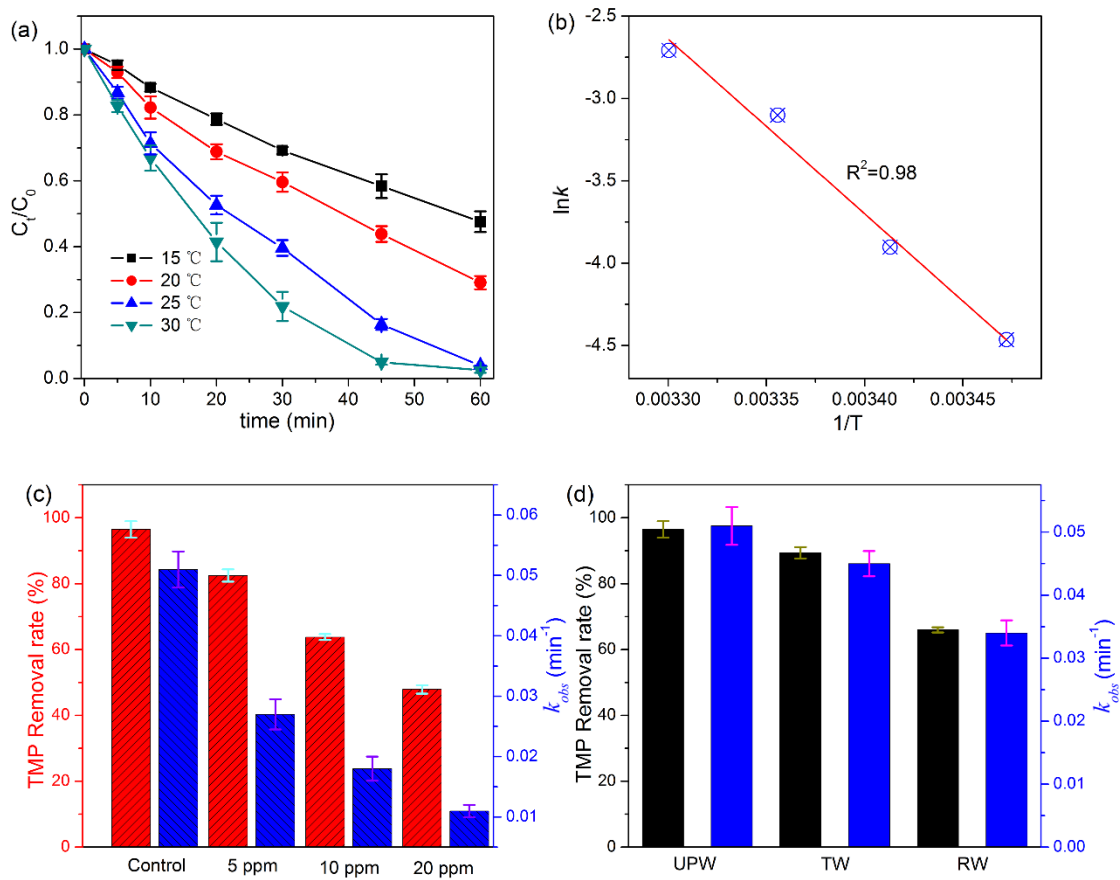


Fig. 6

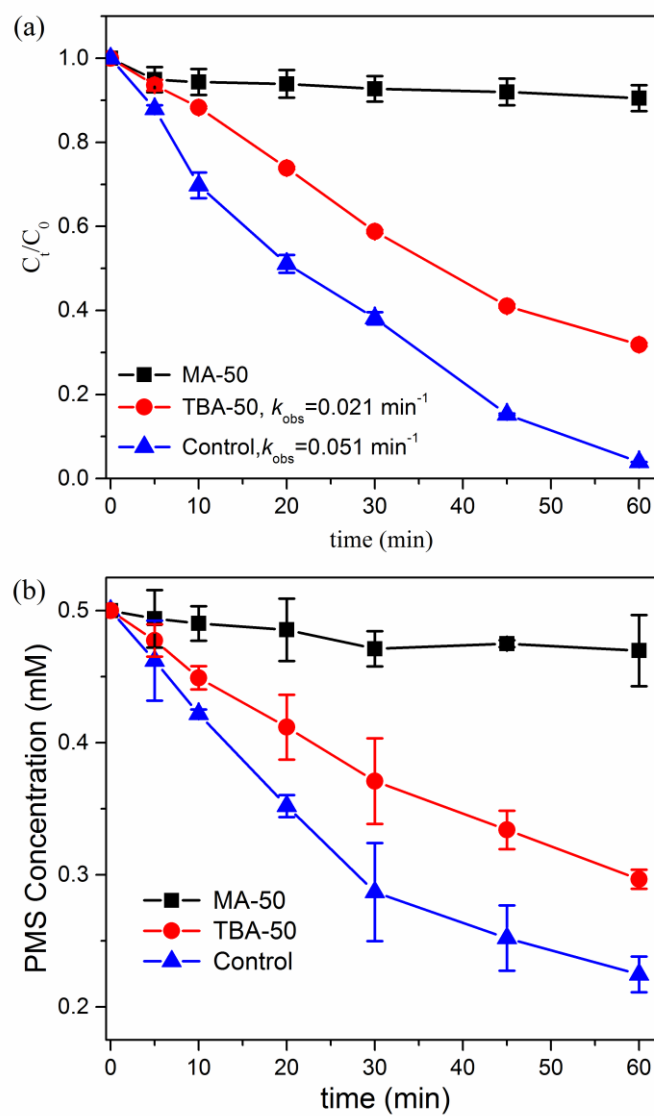




Fig. 7

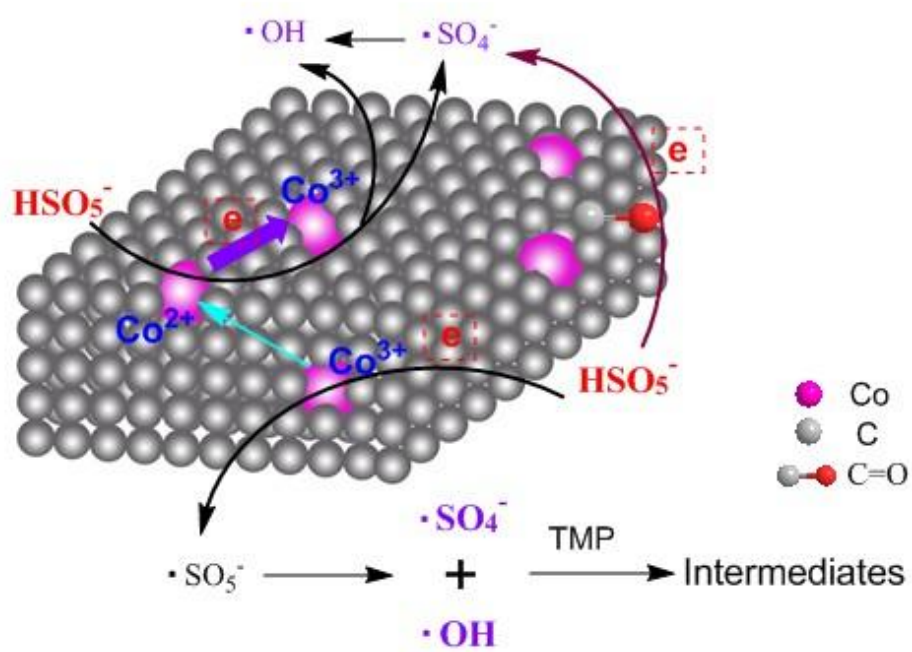
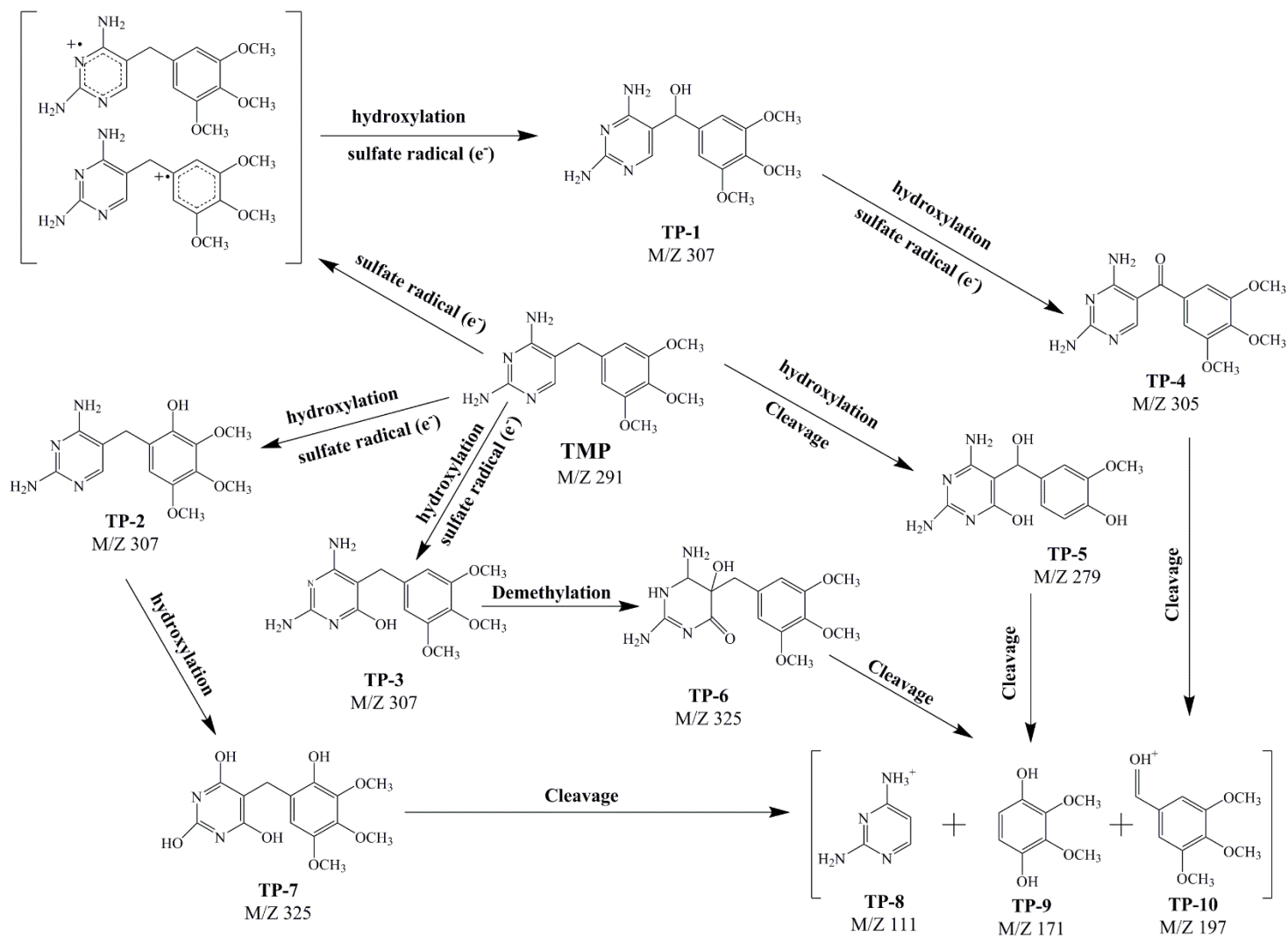


Fig. 8



ACCEPTED

## Highlights

- Novel carbon-supported Co (CS-Co) composites were synthesized by carbonization process from a saturated cationic resin.
- The composites exhibit excellent PMS activation for TMP degradation.
- Scavenging tests confirmed  $\cdot\text{SO}_4^-$  and  $\cdot\text{OH}$  were the dominant reactive radicals.
- Normalized steady-state concentrations of  $\cdot\text{SO}_4^-$  and  $\cdot\text{OH}$  were calculated.
- TMP degradation pathways were proposed based on the identified intermediates.

ACCEPTED MANUSCRIPT

